Photochemistry and Photobiology Vol. 54, No. 6, pp. 937–948, 1991
Printed in Great Britain.

0031-8655/91 $03.00+0.00

STRUCTURE OF BACTERIORHODOPSIN AND *in situ* ISOMERIZATION OF RETINAL: A MOLECULAR DYNAMICS STUDY*

M. NONELLA, A. WINDEMUTH and K. SCHULTEN†
Beckman Institute and Department of Physics, University of Illinois, Urbana, IL 61801, USA

(*Received* 23 *April* 1991; *accepted* 11 *June* 1991)

Abstract—Henderson's model of the structure of bacteriorhodopsin has been completed by adding the missing loop regions and by subsequent energy minimization and equilibration (for about 100 ps) at 300 K. Analysis of the structure during a later 20 ps molecular dynamics run showed no significant deviations from the Henderson model. *In situ* isomerization reactions of the retinal chromophore in bacteriorhodopsin have then been simulated to investigate the chromophore protein interaction for the three isomerization reactions: (i) all-*trans* → 13-*cis*; (ii) all-*trans* → 13,14-*dicis*; and (iii) all-*trans* → 13,15-*dicis*. We find that reaction (iii) which accompanies dark-adaptation of bacteriorhodopsin can proceed in the binding site without any sterical hinderance and involves negligible motions of the covalently bound Lys-216 and other side groups. Reaction (ii) exhibits a somewhat larger but still small energy barrier and involves little rearrangement of Lys-216 and the protein backbone. Reaction (i) experiences a sterical impediment amounting to more than 10 kT at physiological temperatures and also induces significant structural changes at the binding site. Our simulations also reveal that reaction (ii) as a photo-isomerization process can be completed within about 400 fs, whereas reaction (i) requires longer times for completion. Reaction (i) is also accompanied by a co-rotation of the 14—15 bond by 150° (even when a torsional barrier of 20 kcal/mol is imposed to impede rotation of the 14—15 bond) such that photoreactions (i) and (ii), in effect, lead to very similar final geometries. Isomerization (ii) can readily explain the pump mechanism of bacteriorhodopsin: the sequential, thermal back-reaction 13,14-*dicis* → 13-*cis* → all-*trans* can be acid–base catalyzed, *i.e.*, coupled to deprotonation and reprotonation of retinal's Schiff base nitrogen. The orientation of retinal is such that Asp-85 can act as the acceptor and Asp-96 as the (indirect) donor. The thermal back-reaction 13,14-*dicis* → all-*trans* can be coupled to vectorial Cl^- ion transport as well.

INTRODUCTION

Bacteriorhodopsin is the light-driven proton pump of the purple membrane of *Halobacterium halobium* (Oesterhelt and Stoeckenius, 1973; Oesterhelt, 1976; Henderson, 1977). Its function supports Mitchell's hypothesis of chemiosmotic coupling between redox reactions and adenosine triphosphate (ATP) synthesis in membranes (Mitchell, 1961).

The light absorbing chromophore of bacteriorhodopsin is all-*trans* retinal (Lin and Mathies, 1989) which is bound to Lys-216 through a Schiff base linkage. In contrast to all-*trans* retinal in solution, which is in a 6-s-*cis* conformation (Honig *et al.*, 1971), the chromophore in bacteriorhodopsin is found in a 6-s-*trans* conformation (Harbison *et al.*, 1985; Lin and Mathies, 1989). In the light-adapted state its absorption maximum is at 568 nm. After light excitation of the chromophore a pump cycle is initiated which involves several intermediates distinguishable through their absorption spectra. During this cycle retinal undergoes isomerization reactions and changes its protonation state, such that one proton per absorbed photon is pumped from the cytoplasmic side across the membrane to the extracellular medium (Lozier *et al.*, 1975). The light-induced primary step of this cycle, $BR_{568} \rightarrow H \rightarrow I_{<500\ nm} \rightarrow J_{625} \rightarrow K_{610}$, is extremely fast, with a time constant of about 3 ps to reach K (Dobler *et al.*, 1988; Mathies *et al.*, 1988). Knowledge about the nature of the first intermediate is essential for any understanding of the mechanism of bacteriorhodopsin, for it is the coupling of the thermal back-reaction to protonation and deprotonation reactions which constitutes proton pumping.

Several models for the primary photoreaction of the pump cycle have been proposed, the main models postulating a 13-*cis* (Fodor *et al.*, 1988a) and a 13,14-*dicis* photo-isomerization (Schulten and Tavan, 1978; Schulten, 1978; Orlandi and Schulten, 1979; Schulten *et al.*, 1984). Depending on the postulated isomeric state reached in the primary photoreaction, the models differ mainly as follows: one class of models requires that through a protein conformational change a proton is moved from a site in contact with the cytoplasmic medium to a site in contact with the extracellular space; the other class of models states that retinal through isomerization reactions moves a proton between such sites. Of course, retinal and protein may also act in concert to move the protons between suitable sites

*Dedicated to Professor Walther Stoeckenius on his 70th birthday.
†To whom correspondence should be addressed.

or to change the connectivity between sites to the intracellular and extracellular media.

Unfortunately, the exact isomeric states of retinal in most of the intermediates involved in the photocycle, among them K_{610} and L_{550}, are not known and it is not possible yet to discriminate between the models. Recent experimental results and quantum chemical investigations appear to be consistent with a 13-*cis* geometry (Smith *et al.*, 1986; Fodor *et al.*, 1988b) as well as with a 13,14-*dicis* conformation (Fahmy *et al.*, 1989; Grossjean *et al.*, 1989) for the L_{550} intermediate. In the deprotonated state M of the photocycle, which absorbs at 412 nm, a 13-*cis* conformation of retinal has been determined unequivocally (Pettei *et al.*, 1977; Aton *et al.*, 1977).

Quantumchemical calculations have shown that properties of the protonated Schiff base such as its electronic absorption spectrum (Nakanishi *et al.*, 1980), torsional barriers (Orlandi and Schulten, 1979; Schulten *et al.*, 1984; Oesterhelt *et al.*, 1986), and vibrational frequencies (Grossjean *et al.*, 1990) can be influenced strongly by charged groups in the vicinity of the conjugated system as well as by protonation and deprotonation of the Schiff base retinal.

Models for the mechanism of bacteriorhodopsin's pump cycle so far have been developed without knowledge of the structure of the protein. The first atomic model of bacteriorhodopsin has only recently become available (Henderson *et al.*, 1990). Two-dimensional crystals of bacteriorhodopsin allowed the determination of the protein's electron density using high-resolution electron cryo-microscopy, providing a resolution of 3.5 Å in the membrane plane and approximately 10 Å perpendicular to this plane. These data together with information on the sequence enabled Henderson to determine the positions of all amino acid residues in the helical parts of the protein and to construct and refine a structure at the atomic level. In the present study this structure has been taken as the starting point for a moleculary dynamics investigation of bacteriorhodopsin and of the isomerization reactions of its retinal chromophore. The Henderson structure, containing only the helical parts of the protein, has been completed to the full peptide chain. This completed structure has then been equilibrated and compared to the original one. The equilibrated structure enabled us to simulate possible isomerization reactions of Schiff base retinal *in situ* and to investigate the interactions between protein and retinal during these isomerization reactions.

MATERIALS AND METHODS

The structure provided by Henderson *et al.* (1990) describes only the helical part of bacteriorhodopsin; no coordinates for the atoms of the interhelical loop regions are provided. Rather than using only the part of the protein described by Henderson and applying artificial constraints to keep the protein intact, we opted for an inclusion of these missing loop regions to obtain a structurally stable protein. The simulated annealing procedure described below was used to determine plausible and relaxed configurations for the loop regions that do not give rise to unnatural forces disturbing the overall structure.

To complete a loop between two helices we first isolated the two residues at the ends of the helices to be connected (anchor residues) and inserted the chain of residues corresponding to the loop sequence between them. This was done using the interactive molecular graphics program QUANTA (Polygen, 1988) on a Silicon Graphics workstation. Each loop was then subjected separately to several cycles of minimization, heating to 2000 K, and 2 ps of equilibration. Only the loop residues and the two anchor residues were included in these simulations and the positions of the anchor residues were kept at fixed positions at all times. The pre-equilibrated loops were then added to the protein and minimized, still keeping the helical part of the protein rigid.

The completed loop structures were minimized at this stage together, equilibrated at 2000 K, and finally cooled down to 300 K through coupling protein motions to a heat bath by means of the *t-coupling* method (friction coefficient = 0.1 fs^{-1}) (Berendsen *et al.*, 1984). The temperature of the heat bath was lowered by 25 K every 100 fs until the final temperature of 300 K was reached. During this procedure, the helical part of the structure provided in Henderson *et al.* (1990) was kept rigid.

After this procedure the helic constraints were lifted and the whole protein was energy minimized. In order to prevent large structural changes caused by strongly interacting side chains the minimization was carried out in two steps, a first step with the protein backbone atoms of the helical portion still constrained to their initial positions, and a second step without any constraints. The resulting minimized structure was then heated to 300 K and equilibrated at constant temperature for 20 ps, followed by a free dynamics simulation of 40 ps.

For the procedures described above standard protonation states were assumed for the amino acids as defined in the X-PLOR (Brünger, 1988) topology definitions. In bacteriorhodopsin it is known that the *in situ* p*K*-value of Asp-96 is changed by the protein environment and it has been shown that this group is neutral in the state BR_{568} (Gerwert *et al.*, 1989; Braiman *et al.*, 1988). For this reason, Asp-96 was protonated after the above procedures and an additional equilibration of 12 ps and a molecular dynamics simulation of 20 ps was performed.

All dynamics simulations used to prepare a complete structure of bacteriorhodopsin were carried out using the program X-PLOR (Brünger, 1988), which implements the CHARMM (Brooks *et al.*, 1983) force field. For the adiabatic isomerization calculations described below we used the molecular dynamics program MD implemented on the Connection Machine (Windemuth and Schulten, 1991). This program, like X-PLOR, employs the CHARMM force field. The program allowed us to modify the force field for specific degrees of freedom as necessary to induce isomerization reactions of retinal.

Partial charges for the protonated Schiff base have been determined using the program package AMPAC (Dewar and Stewart, 1986). Force constants for the Schiff base were derived from molecules with similar chemical structures for which parameters are available in CHARMM or X-PLOR. The geometry of retinal was assumed to be all-*trans* (Lin and Mathies, 1989).

The potential which governs the motion of dihedral angles in CHARMM is

$$E_{dih} = k_{dih}[1 + \cos(n\phi + \delta)], \quad (1)$$

with $n = 2$ (periodicity) and $\delta = 180°$ (phase factor) in the case of the planar, all-*trans* retinal chain conformation.

For the purpose of our simulations it is more convenient to introduce the angle of lowest energy $\phi_0 = -\delta/n$ instead

of the phase factor δ. Equation (1) then reads

$$E_{dih} = k_{dih}[1 - \cos n(\phi - \phi_0)] \quad (2)$$

The force constant of a double bond has been set to k_{dih} = 23.5 kcal/mol to account for a torsional barrier of 2 k_{dih} = 47 kcal/mol. For the torsional barrier of single bonds in the retinal chromophore a barrier of 20 kcal/mol was assumed implying a force constant k_{dih} = 10 kcal/mol. This latter value helped to keep the retinal chromophore planar during the simulation. The high value is consistent with quantum chemical studies of single-bond isomerization barriers of protonated Schiff base polyenes (Orlandi and Schulten, 1979; Schulten *et al.*, 1984).

Cis–trans isomerizations of retinal have been induced in three different ways, referred to as methods A, B and C.

Inducing isomerization through a slow change of torsional potentials—Method A. Method A provides a guiding force by adiabatically varying the angle of lowest energy ϕ_0 of the affected dihedrals during the simulation. This was realized by choosing the angle ϕ_0, time-dependent during the simulation period of length τ_s

$$\phi_0(t) = \left(1 - \frac{t}{\tau_s}\right)\phi_i + \frac{t}{\tau_s}\phi_f. \quad (3)$$

ϕ_i and ϕ_f are the initial and final dihedral angles. ϕ_i was always chosen to be 180°, as the retinal is initially in the all-*trans* conformation. A final angle ϕ_f = 0° (complete *trans–cis* isomerization) was chosen for those bonds that were to be isomerized.

Actually, in the following simulations we have subjected three torsional angles to shifts of the torsional minima. To describe the corresponding variation of the potential we employ Eq. (3) simultaneously on one or two of a set of three angles. This can be described in vector notation as

$$\vec{\phi}_0(t) = \left(1 - \frac{t}{\tau_s}\right)\vec{\phi}_i + \frac{t}{\tau_s}\vec{\phi}_f \quad (4)$$

where $\vec{\phi}_0 = (\phi_{0,\,13-14}, \phi_{0,\,14-15}, \phi_{0,\,15-N})^T$ is a three-component vector, $\phi_{0,\,13-14}$ denoting the initial minimum of the 13—14 bond of retinal *etc.*, and where $\vec{\phi}_f$ is defined in an analogous way. For the simulations considered below $\vec{\phi}_0 = (180°, 180°, 180°)^T$, holds *i.e.* retinal is always in an initial all-*trans* state. For the transformation (i) all-*trans* → 13-*cis*, (ii) all-*trans* → 13,14-*dicis*, and (iii) all-*trans* → 13,15-*dicis*, one has: (i) $\vec{\phi}_f = (0, 180°, 180°)^T$; (ii) $\vec{\phi}_f = (0, 0, 180°)^T$; and (iii) $\vec{\phi}_f = (0, 180°, 0)^T$.

The simulation time τ_s must be sufficiently long to ensure that the change in the potential surface is adiabatic, *i.e.*, that all degrees of freedom should remain close to equilibrium. A criterion for adiabaticity can be derived from the thermal energy of the torsional potential of a bond, which, according to the equipartition theorem, is

$$\Delta E_{therm} = \frac{1}{2}k_B T \approx 0.3 \text{ kcal/mol},$$

since the potential is locally ($\phi \approx \phi_0$) harmonic. The frequency of torsional vibrations in the high-barrier double bonds can be estimated by neglecting the coupling between neighboring bonds and using the harmonic approximation, yielding (k_{dih} = 23.5 kcal/mol)

$$\omega = \sqrt{\frac{n^2 k_{dih}}{mR^2}} \approx \frac{1}{18 \text{ fs}}.$$

Here, the carbon atom mass m = 12 a.m.u. was used and a typical atomic distance of R = 1 Å was assumed for the distance of that atom from the torsion axis.

Thus, the torsional vibrations have a period $2\pi/\omega$ of approximately 100 fs, and a perturbation of the corresponding potential surface is adiabatic when the change ΔE_{pot} applied during a time interval Δt = 100 fs is much smaller than the thermal energy ΔE_{therm}. In this case, the change in the potential surface is caused by a change

$$\Delta\phi_0 = \frac{\Delta t}{\tau_s}(\phi_f - \phi_i)$$

of the equilibrium angle ϕ_0, leading to

$$\Delta E_{pot} = E_{dih}(\phi, \phi_0 + \Delta\phi_0) - E_{dih}(\phi, \phi_0)$$
$$\approx 2\,k_{dih}\left(\frac{\Delta t}{\tau_s}\right)^2(\phi_f - \phi_i)^2$$

This value must be significantly smaller than $\frac{1}{2}\,k_B T$, a condition which implies

$$\tau_s \gg 2\Delta t(\phi_f - \phi_i)\sqrt{\frac{k_{dih}}{k_B T}} \approx 0.7 \text{ ps}. \quad (5)$$

Accordingly, we chose τ_s = 10 ps for the simulation time. During this time the bonds complete over 70 torsional oscillations around ϕ_0. This high number implies that retinal can adjust well to the shift of potential minima during the simulation.

The ability of retinal to isomerize is significantly restricted by the surrounding protein, mostly due to sterical hindrance arising from the tightly packed amino acid residues in the vicinity of the chromophore. To investigate the effect of this hindrance on the reaction barriers for different isomerization reactions it is useful to analyze the amount of distortion that retinal is subjected to during the forced isomerization process. A good measure for this distortion is the deviation of the actual dihedral angle ϕ from the equilibrium value $\phi_0(t)$ during the simulation. We recorded and analyzed this deviation and the corresponding dihedral angle potentials given by Eq. (2) for the angles 13—14, 14—15 and 15—N to quantify the chromophore–protein interaction during the simulations.

The information provided by the quantities $\phi_{bond} - \phi_{0,\,bond}$ and the corresponding potentials $E_{dih,\,bond}(\phi_{bond}, \phi_{0,\,bond}) - E_{dih,\,bond}(\phi_{0,\,bond}, \phi_{0,\,bond})$ for the various "bonds" of retinal can be illustrated through an analogy: assume a man walking his dog using an elastic rubber band as a leash. The man guides the dog "adiabatically" if he walks slowly such that the dog can easily follow while still exploring his surroundings. One can then use the length of the rubber band, or the elastic energy stored in the rubber band, to obtain information about the effect of the surroundings on the dog. During much of the walk the length as well as the energy will vary randomly around a mean value. However, there might be instances along the walk when the attention of the dog was particularly engaged with objects such that length and energy of the rubber band increased significantly. One may equate then the maximum energy occurring in the leash at such instances to energy barriers erected by the surroundings against the dog's further motion. If one likens the leash to the potential $E_{dih,\,bond}$, the time variation of $\phi_{0,\,bond}$ to the walking man, then obviously $\phi_{bond} - \phi_{0,\,bond}$ and $E_{dih,\,bond}(\phi_{bond}, \phi_{0,\,bond}) - E_{dih,\,bond}(\phi_{0,\,bond}, \phi_{0,\,bond})$ provide us with information about the resistance which retinal experiences along the various isomerization pathways.

Inducing isomerization through sudden change of dihedral potential—Method B. In a second set of simulations, referred to as method B, the potentials (Eq. 2) governing the dihedral angles have been changed *instantaneously* such that the all-*trans* conformations became unstable and the respective *cis*-positions stable. In the case of an isomerization around a particular bond the potential adopted is

$$E_{dih} = k_{dih}[1 - \cos(\phi)]. \quad (6)$$

This potential has a maximum at the all-*trans*-position ϕ = 180° and a minimum at the *cis*-position ϕ = 0°. Two potentials of this type for two bonds, *i.e.*, for the 13—14,

14—15 or for the 13—14,15—N bonds, would induce the concerted isomerizations all-*trans* → 13,14-*dicis* and all-*trans* → 13,15-*dicis*, respectively.

Subsequent to the change of potentials the simulation monitors the dihedral angles of retinal and, in particular, measures the times to complete the isomerizations. The latter time provides a measure for the resistance that the protein poses to the isomerization reactions enforced and can be compared with experimentally observed reaction times.

The reaction time of the primary process in the photocycle, *i.e.*, the time needed to reach state J_{625} on the potential energy surface of the electronic ground state (Mathies *et al.*, 1988) is very short (0.5 ps) (Dobler *et al.*, 1988). This implies that the crossing between the potential energy surfaces of the S_0 and S_1 states of retinal occurs close to the maximum of the ground-state potential surface (Schulten, 1978). Thus, the unstable state used as the initial state is a reasonable model for retinal directly after the decay of the excited state.

We must point out that no attempt has been made in the present study to describe the potential energy surface for the first excited state S_1. A few points on the S_1 surface have been determined in Orlandi and Schulten (1979) within a CNDO description coupled to a CI treatment involving single and double excitations. Method B assumes that crossing from the S_1 surface to the S_0 surface is fast and that, therefore, the photo-isomerization can be described by a single potential surface.

Inducing isomerization through stepwise (10°) changes of dihedral potentials—Method C. In order to monitor structural changes occurring near the binding site of bacteriorhodopsin during the various isomerization reactions we have varied the equilibrium positions ϕ_0 of the dihedral angles involved in a particular isomerization in steps of 10°. For each configuration a 2 ps simulation was carried out: 1 ps to allow the changed configuration to equilibrate and 1 ps to average the resulting structure. These simulations allow one to visualize which protein structural changes accompany the different isomerization reactions.

RESULTS

Structure

We want to compare first the average structure of BR_{568} resulting from a 20 ps dynamics simulation to the Henderson structure (Henderson *et al.*, 1990). Figure 1 shows the backbone of the Henderson and the averaged simulated structures of the helical portion of the protein. One can note that the structures match well and also that the protein did not expand during the simulation. This result is very important for two reasons: first, it indicates that the structure fitted to the data obtained by high resolution electron microscopy is indeed close to a minimum energy conformation on the energy landscape; and second, the result suggests that the structure remains stable during a free molecular dynamics simulation, *i.e.*, remains stable without applying any constraints and without including membrane or water.

The mean deviation of the average simulated structure from the Henderson structure, considering only the protein backbone of the helical portions of bacteriorhodopsin, corresponds to a root-mean-square (RMS) value of 2.85 Å. This value seems quite large when compared to RMS values observed for the dynamics of single structures, *e.g.*, the one obtained for the photosynthetic reaction center (Treutlein *et al.*, 1988; Nonella and Schulten, 1991). It must be taken into account, however, that the original structure is not comparable in resolution to an x-ray crystallographic structure and that the protein is relatively small and was simulated without membrane and water.

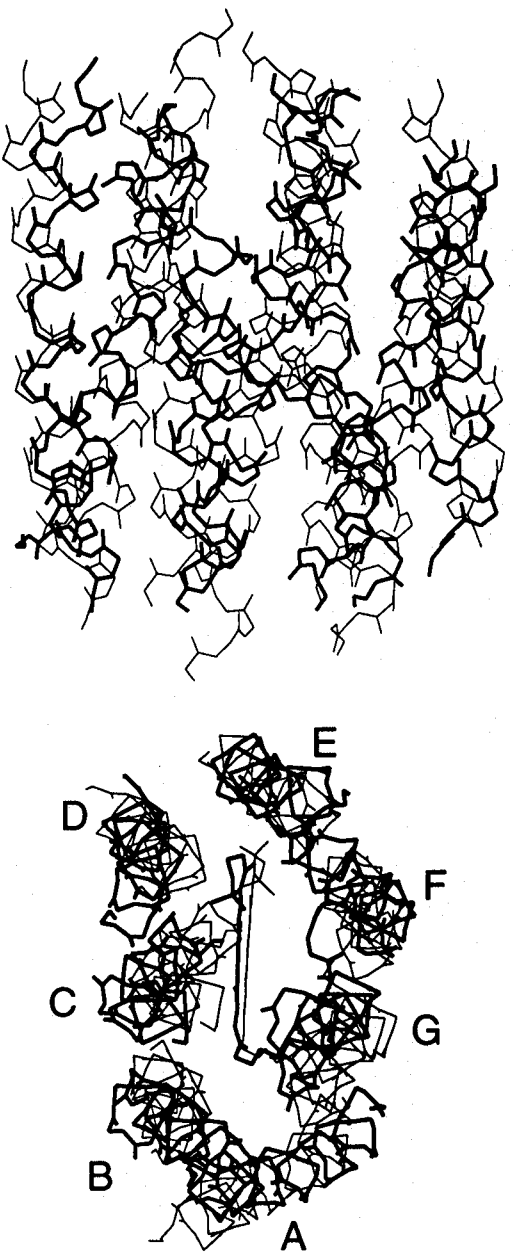

Figure 1. Overlaid average simulated (thick line) and experimental (thin line) structure of the backbone of bacteriorhodopsin. Only the part of the structure reported in Henderson *et al.* (1990) is shown. The top represents a side view of the protein and the bottom shows a view from the periplasmic side down the α-helices.

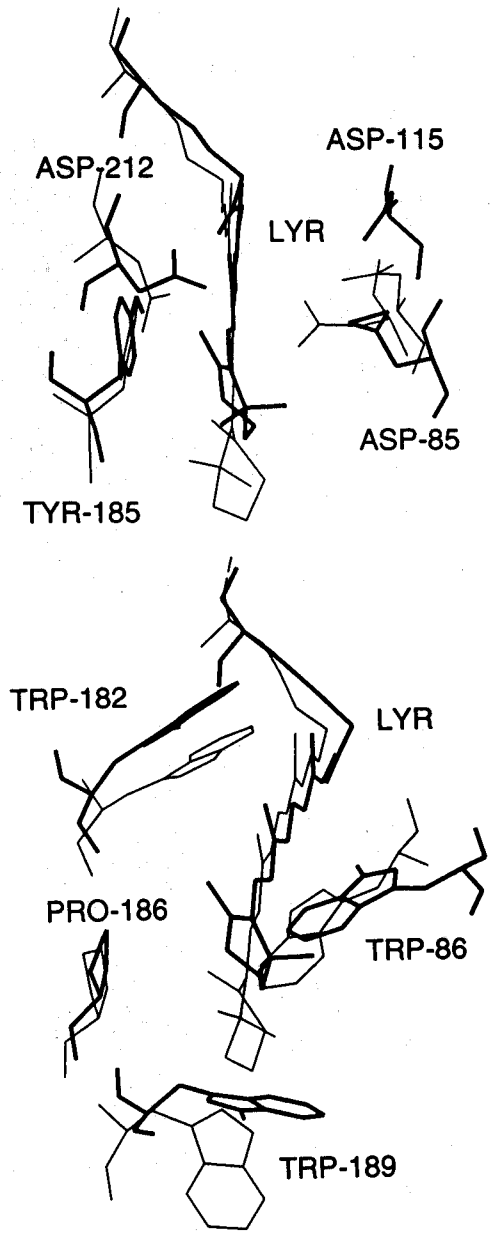

Figure 2. Overlaid average simulated (thick line) and experimental (thin line) structure of the region close to the Schiff base retinal complex. The top shows the lysine–retinal complex and aspartic acids 212, 115, and 85 and tyrosine 185. The bottom shows again the lysine–retinal complex and trypsines 86, 182, 189 and proline 186 which are "sandwiching" the conjugated system of retinal.

Figure 2 shows the region close to the Schiff base retinal complex, comparing again the Henderson and the averaged simulated structures. The most prominent differences concern the two aspartic acids 85 and 212. Asp-212 significantly moves towards the Schiff base proton, whereas Asp-85 moves away from it. Asp-85, Asp-212, and Asp-115 are all assumed to be negatively charged (unprotonated) in our simulations. It has been suggested, however,

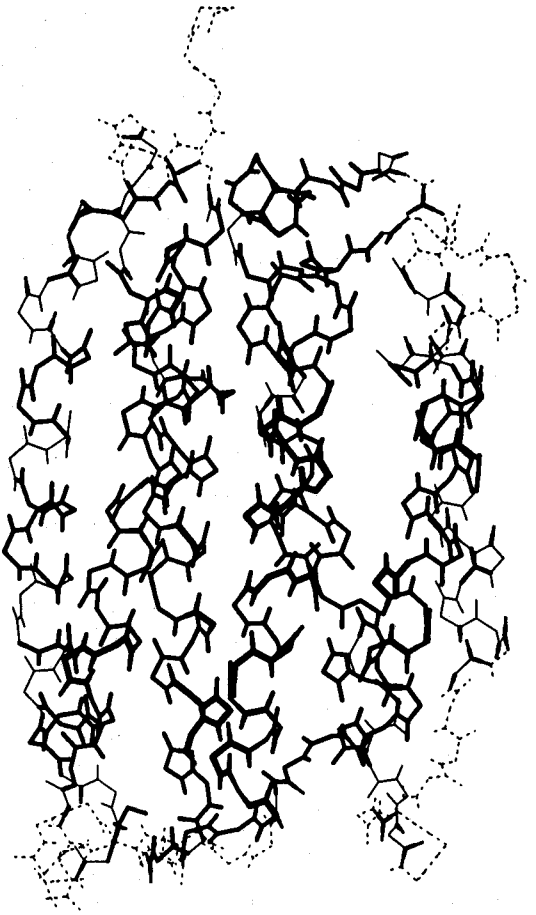

Figure 3. Mobilities of the backbone atoms of bacteriorhodopsin. The RMS values are represented as follows: thin dashed line, RMS >0.8 Å; thin line, 0.8 Å < RMS <0.6 Å; medium line, 0.6 Å < RMS <0.5 Å; thick line, 0.5 Å < RMS <0.4 Å.

that Asp-115 should be protonated in BR_{568} (Gerwert *et al.*, 1989; Braiman *et al.*, 1988). Asp-212 is bound to the same helix as Lys-216 and, therefore, is constrained to stay in the vicinity of the Schiff base. The displacement of Asp-85 is then due to electrostatic repulsion between the two aspartic acids which are both assumed to carry a negative charge. This structural change is most important since Asp-85 is believed to take up the proton of retinal's Schiff base after the primary photoreaction.

We have also determined the RMS deviations of the atoms in our equilibrated structure. In the isotropic harmonic model the calculated mean-square atomic fluctuations are directly related to the experimental temperature factor B_i according to

$$B_i = \frac{8}{3}\pi^2 < \Delta r_i^2 >.$$

The calculated RMS values for all the backbone atoms are presented in Fig. 3. The RMS values of most of the atoms belonging to the helical structure lie between 0.4 and 0.5 Å, corresponding to *B*-

values between 10.7 and 13.3 Å^2. These values are in good agreement with the experimental result of a *B*-factor of about 12.4 Å^2 for an α-helix and with typical theoretical results between 11.3 and 11.7 Å^2 (Karplus, 1986). Most of the atoms belonging to the loop regions exhibit larger mobilities, in agreement with the experimental findings that a determination of the structure of these parts of the protein was not possible at a reasonable accuracy, presumably due to the high flexibility of the atoms involved as well as to the two-dimensional nature of the bacteriorhodopsin crystals used in the structural analysis.

Isomerizations induced according to method A

We have simulated the isomerization reactions (i) all-*trans* → 13-*cis*, (ii) all-*trans* → 13,14-*dicis* and (iii) all-*trans*→ 13,15-*dicis* according to method A described above. The method enforces these isomerizations by prescribing a time-dependence of the angles of torsional stability $\phi_{0,\,\mathrm{bond}}$ (bond = 13—14, 14—15, 15—N) according to Eq. (4). The structure of bacteriorhodopsin and, in particular, of retinal adjusts to the changed dihedral potential functions. Figure 4 presents the angles $\phi_{13-14}(t)$, $\phi_{14-15}(t)$ and $\phi_{15-N}(t)$ resulting from this adjustment. One can recognize that the method does indeed induce the desired isomerizations of retinal.

The 13-*cis* isomerization presented in Fig. 4(a) was proposed for the primary step of the photocycle by Fodor *et al.* (1988a). The significant deviation of the 13—14 dihedral angle from its equilibrium value indicates a high degree of resistance to the isomerization caused by the retinal–protein interaction. In addition, the deviation of the 15—N dihedral angle demonstrates that the torsional strain caused by the single isomerization is not localized, but spreads over several bonds. The reader should bear in mind that according to method A the simulations in the present case shift $\phi_{0,\,13-14}$ from 180° to 0° *while attempting to prevent a torsion around the 14—15 bond* through a 20 kcal/mol barrier.

The 13,14-*dicis* isomerization presented in Fig. 4(b) was proposed by Schulten and coworkers (Schulten and Tavan, 1978; Schulten, 1978; Orlandi and Schulten, 1979; Schulten *et al.*, 1984). The small deviation of the 13—14 dihedral angle from its equilibrium value as well as the absence of any other significant deviations imply that this isomerization is much more compatible with the constraints imposed on the chromophore by its tight binding pocket.

The 13,15-*dicis* isomerization presented in Fig. 4(c) was simulated as a control to check the validity of the method. This isomerization, which due to an internal isomerization barrier requires about an hour to complete, is not thought to be involved in the primary photoreaction, but to occur spontaneously in the transition from the active to the dark-adapted state. From geometrical considerations almost no interference from the protein is expected for this isomerization. The reason is that two parallel bonds, *i.e.*, the 13—14 and the 15—N bonds, are rotated in opposite directions, the rotations largely compensating each other and giving rise to a so-called *bicycle pedal* motion which requires only a small reaction volume. This expectation is clearly borne out by the results in Fig. 4(c), which do not show any significant deviation of the angles $\phi_{\mathrm{bond}}(t)$ from their equilibrium values $\phi_{0,\,\mathrm{bond}}(t)$. In addition, the small deviation also indicates that the changes in the dihedral angle potential are slow enough for the angles to remain in equilibrium while following the guiding forces. This demonstrates that the potential change prescribed in method A is indeed slow enough for the protein structure to continually adjust.

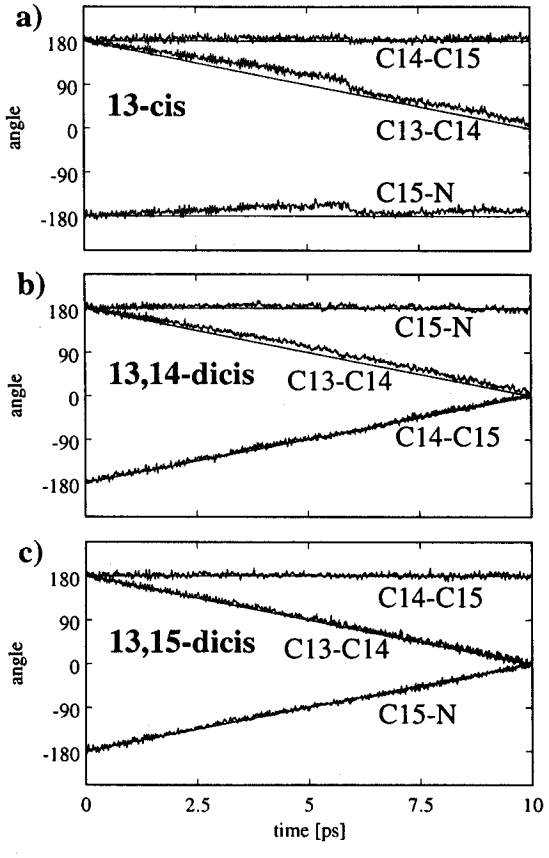

Figure 4. Dihedral angles (designated by their respective bonds) of retinal during a 10 ps molecular dynamics simulation with an adiabatic guiding force to induce the three different isomerizations according to method A. The straight lines represent the angles of lowest energy $\phi_{0,\,13-14}(t)$, $\phi_{0,\,14-15}(t)$ and $\phi_{0,\,15-N}(t)$ as prescribed by the molecular dynamics force field. The fluctuating lines present the angles $\phi_{13-14}(t)$, $\phi_{14-15}(t)$ and $\phi_{15-N}(t)$ during the simulation.

Figure 5 presents the conformational energy introduced in the Materials and Methods section. The behavior of the conformational energies support the conclusions above except that the differ-

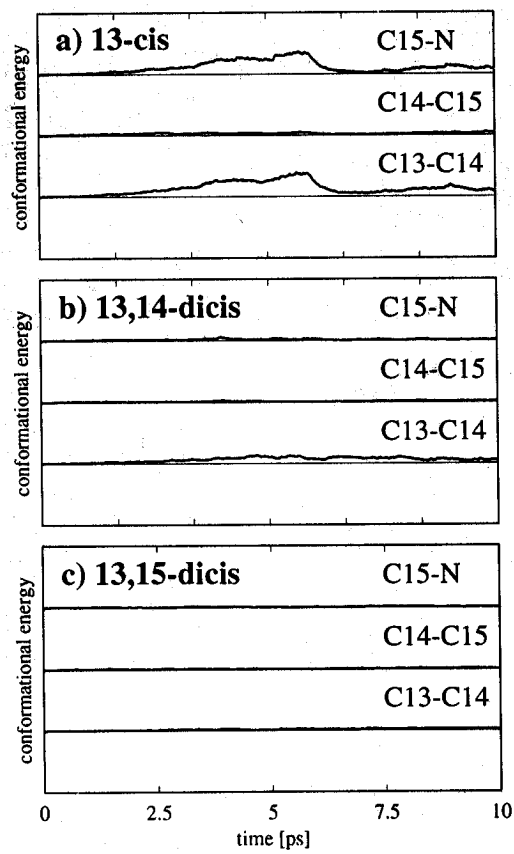

Figure 5. Conformational energies of the three relevant dihedral angles $\phi_{13-14}(t)$, $\phi_{14-15}(t)$ and $\phi_{15-N}(t)$ are shown for each of the three isomerizations (i)–(iii) performed. The thin baselines are separated by 11 kcal for the $\phi_{13-14}(t)$ and $\phi_{15-N}(t)$ dihedral angles and by 5 kcal for the $\phi_{14-15}(t)$ dihedral angle, which is ¼ of the torsion barrier height for the corresponding dihedral angle. Values have been averaged in a gliding average over a time window of 0.2 ps.

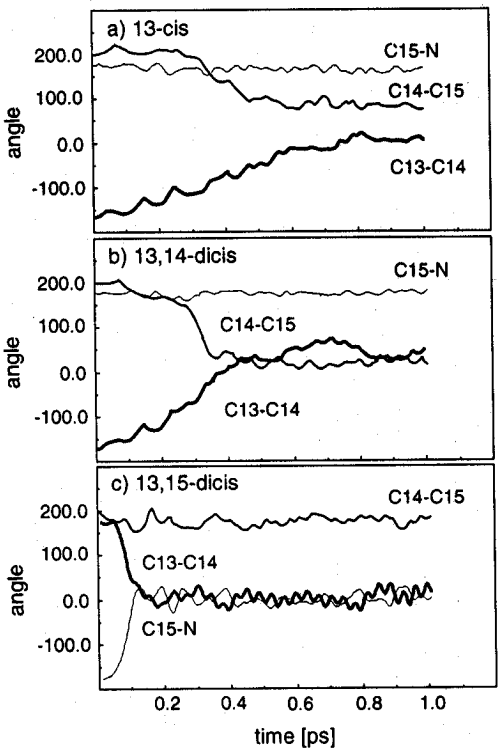

Figure 6. Time development of selected dihedral angles after the potential function of one or two dihedrals has been changed in order to start a simulation on the saddle-point of the corresponding isomerization. (a) Corresponds to the primary step according to the C–T model (Fodor *et al.*, 1988a), *i.e.*, isomerization (i). (b) Corresponds to the primary step as suggested in Schulten and Tavan (1978), *i.e.*, isomerization (ii). (c) Describes the isomerization from the light-adapted to the dark-adapted state, which should not be significantly hindered by the protein since it is thermally accessible.

ences between the isomerizations are even more pronounced. (This is simply due to the fact that the energies depend quadratically on $\phi_{bond} - \phi_{0,\,bond}$.) Additionally, the conformational energy values allow us to quantitatively estimate a lower bound for the contribution of the retinal–protein interaction to the potential barrier of a specific isomerization reaction. At the midpoint of the 13-*cis* isomerization the two double bonds 13—14 and 15—N alone experience a combined conformational energy barrier of approximately 10 kcal/mol. The contribution to the potential barrier is likely to be higher than this value since the torsional strain spreads to other degrees of freedom besides the three dihedral angles presented in Fig. 5.

Isomerizations induced according to method B

Figure 6 shows the time development for isomerization processes induced according to method B, *i.e.*, simulated after changing the potential energy surface of the respective bonds instantaneously. Such an instantaneous change models the act of photoexcitation. Figure 6(a) provides the time-dependence of the dihedral angles of the 13—14, 14—15 and 15—N bonds indicating the degree of completion of the all-*trans* → 13-*cis* isomerization. The time needed to reach the new equilibrium conformation is a measure for the energetic hindrance by the protein against this isomerization. The isomerization is completed after about 800 fs. Interestingly, in addition to the enforced isomerization around the 13—14 bond, a rotation of approximately 150° around the 14—15 bond in bacteriorhodopsin is accompanied by a torsion around the 14—15 bond such that the resulting isomer is close to a 13,14-*dicis* conformation.

Figure 6(b) provides the time-dependence of the dihedral angles of the 13—14, 14—15 and 15—N bonds of retinal for an isomerization enforced by an instantaneous change of the potentials for the 13—14 and 14—15 bond angles. The resulting all-*trans* → 13,14-*dicis* isomerization process is less hin-

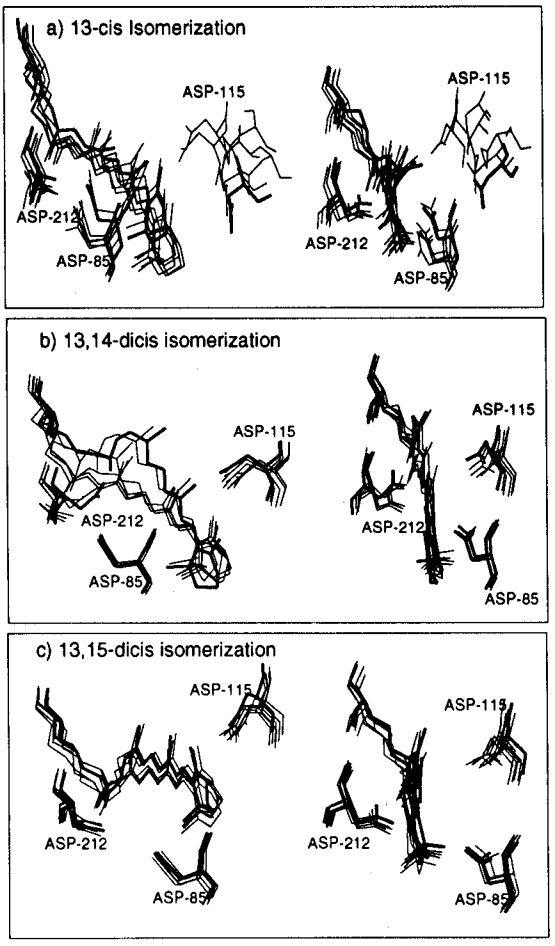

Figure 7. View of averaged geometries of retinal and neighboring amino acid side groups during isomerization reactions induced by stepwise (10°) changes of angles $\phi_{0,\,bond}$ from 180° to 0°. Shown are geometries for $\phi_{0,\,bond}$ = 180°, 150°, 120°, 90°, 60°, 30° and 0°. Thin lines represent starting and intermediate structures and thick lines represent the final structures.

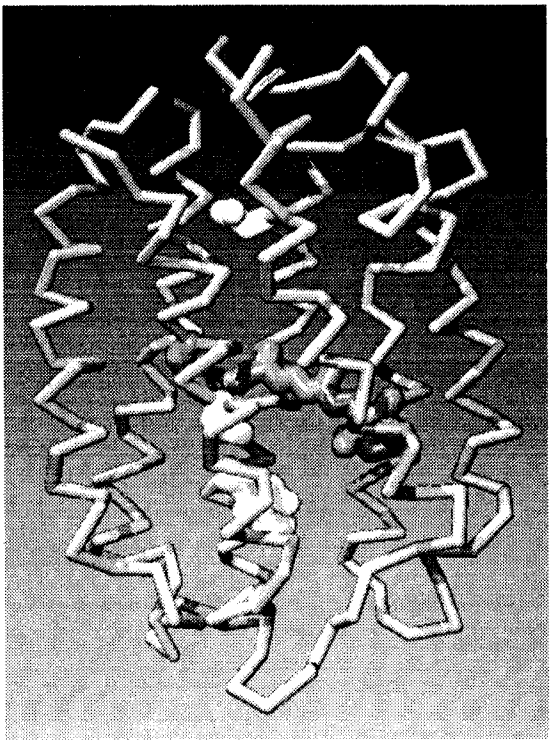

Figure 8. Schematic presentation of the bacteriorhodopsin backbone including the retinal chromophore and some key amino acid side groups shown in white: Asp-212 near the retinal Schiff base with Asp-85 hidden behind it, Asp-96 situated towards the cytoplasmic side (above retinal) and Arg-82 situated towards the extracellular side (below retinal). See also the figure on the outside back cover of this issue of *Photochemistry and Photobiology*.

dered by the protein matrix than the isomerization all-*trans* → 13-*cis*, as reflected by the shorter time needed to reach the new minimum energy conformation (400 fs). It is worth noting that the time needed for this isomerization is close to the experimentally measured reaction time of about 500 fs for this step (Dobler *et al.*, 1988; Mathies *et al.*, 1988), *i.e.*, for the isomerization all-*trans* → J_{625}, the primary step of the photocycle after light excitation.

Figure 6(c) presents the dihedral angles resulting from a simulation describing a *hypothetical* all-*trans* → 13,15-*dicis* photo-isomerization induced according to method B. This isomerization should not be hindered strongly by the protein, as was noted in the last section. This is reflected in Fig. 6(c) which shows that the isomerization is completed within the extremely short time span of 100 fs.

Isomerizations induced by method C

In order to visualize how the three investigated isomerizations of retinal might take place in the tight binding pocket in bacteriorhodopsin several intermediate stages of the isomerization determined according to method C introduced in the Materials and Methods section are presented in Fig. 7. Figure 7 clearly shows that the all-*trans* → 13,15 -*dicis* isomerization (iii) produces the smallest structural changes of all three reactions. A common property of all reactions is a very small displacement of the ring system of retinal. The most prominent displacements occur in the region of the Schiff base. It must be noted that in the presented case of an all-*trans* → 13-*cis* isomerization the Schiff base proton is tilted towards the cytoplasmic side of the protein, *i.e.*, towards the "wrong" direction, whereas an all-*trans* → 13,14-*dicis* isomerization (ii) keeps the proton pointing towards the extracellular side, *i.e.*, towards the "right" direction. In the case of the all-*trans* → 13-*cis* isomerization (i) large displacements of Asp-85 and Asp-115 are induced. This observation indicates that the total protein structure is significantly affected by such isomerization. As argued before, we suggest that the 13-*cis* isomeric state should actually arise for the (second) M-inter-

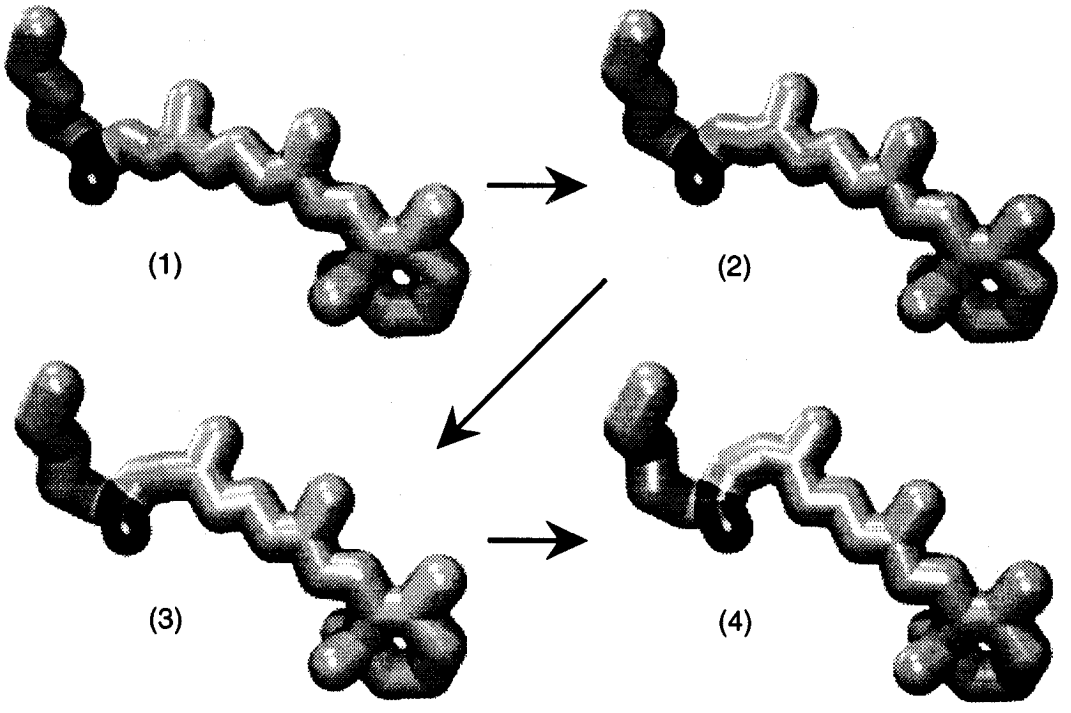

Figure 9. Sequence of retinal conformations during the 13,14-*dicis* isomerization simulation. The retinal molecule with the side chain of Lys-212 covalently bound is shown. The Schiff base nitrogen together with its proton are shown in black.

mediate. In fact, observations have shown a significant change of the protein structure accompanying the L → M transition.

DISCUSSION

In Fig. 8 we present a schematic view of the structure of bacteriorhodopsin which shows the protein's seven α-helices, the retinal chromophore as well as some key amino acid side groups. Figures 9 and 10, below, show the same view of retinal as that presented in Fig. 8. Hence, Fig. 8 serves to relate retinal motion and protonation reactions to the overall structure of bacteriorhodopsin.

The simulations of the complete bacteriorhodopsin after equilibration yielded relatively large RMS deviations of 2.85 Å from the structure of Henderson. The deviations are, however not larger than the lateral resolution of 3.5 Å of the electron density as reported in Henderson *et al.* (1990). This raises the question of whether the equilibrium structure resulting from free molecular dynamics simulation might not fit the experimental data as well as the originally given structure, leading to an opportunity for future research.

It appears to be significant that the time scale of the isomerization reaction as presented in Fig. 6 corresponds rather closely to the measured value of about 500 fs (Dobler *et al.*, 1988; Mathies *et al.*, 1988). We interpret this as evidence that the primary photo-isomerization of retinal proceeds nearly unimpeded by the protein matrix, explaining the apparent preference of the system for an all-*trans* → 13,14-*dicis* isomerization, which requires less space than an all-*trans* → 13-*cis* isomerization.

The results of the simulations presented above are consistent with the model put forward in (Schulten and Tavan, 1978; Schulten, 1978; Orlandi and Schulten, 1979; Schulten *et al.*, 1984), which involves the all-*trans* → 13,14-*dicis* isomerization as the primary isomerization state. This model provides a consistent picture of the sequence of retinal conformations during the pump cycle which emerges from looking at the all-*trans* → 13,14-*dicis* isomerization in the context of the overall protein structure. Figure 9 presents a space-filling model of the sequence of retinal conformations during all-*trans* → 13,14-*dicis* isomerization (ii) induced through method A. It can be seen that the molecule reaches the new isomeric state by means of a minimal motion involving an inversion-type move of C_{13}—H. Actually, the motion entails a slight gliding motion of the β-ionone ring of retinal, an increase of the tilt of the conjugated backbone of retinal, a shift by 1–2 Å of the Schiff base proton towards the cytoplasmic side* and a slight pull on the lysine side chain. The motions described can be recognized

*The reader may note that this motion is opposite to the direction of proton pumping, a behavior which is in agreement with observations of charge shifts in bacteriorhodopsin reported in Keszthelyi and Ormos (1980).

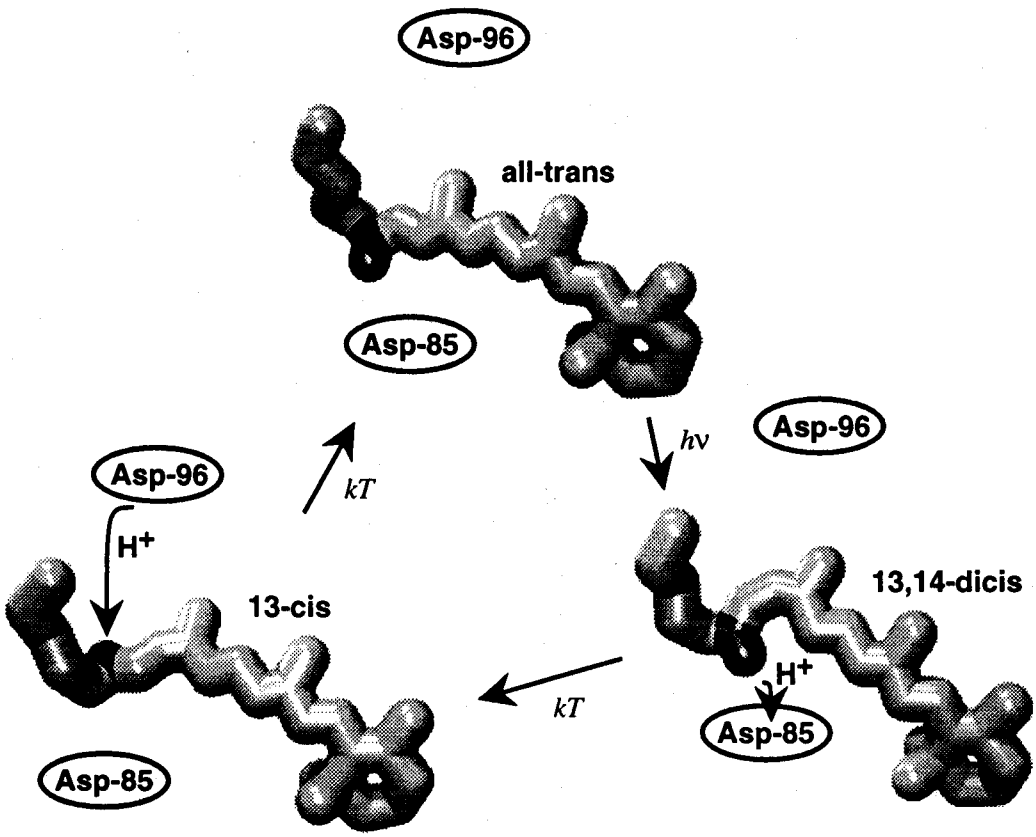

Figure 10. Isomerization states of retinal during the photocycle according to the model discussed in the text. Retinal first undergoes an all-*trans* → 13,14-*dicis* photo-isomerization, bringing the Schiff base into closer contact with the primary proton acceptor Asp-85, the Schiff base proton pointing (down) towards the extracellular side. After deprotonation a thermal relaxation to the 13-*cis* isomerization state occurs, turning the Schiff base around, bringing it closer to the primary proton donor Asp-96 and having the proton binding site pointing (up) towards the cytoplasmic side. After reprotonation retinal isomerizes back to the all-*trans* state. The locations of the side chains Asp-85 and Asp-96 relative to retinal are sketched.

well in Fig. 7(b). The motion also induces a change of the relative position of Asp-212, Asp-85 and the Schiff base nitrogen. A main lesson to be learned from Fig. 9 is that the all-*trans* → 13,14-*dicis* isomerization requires little space and involves the motion of very little mass.

Figure 10 presents the complete sequence of isomerizations and proton transfers consistent with a primary all-*trans* → 13,14-*dicis* photo-isomerization. After the photo-isomerization, shown as the first step in Fig. 10, retinal is trapped in a 13,14-*dicis* geometry since in the ground state of the protonated Schiff base the barriers for rotations around the 13—14 and 14—15 bonds are both relatively large (Orlandi and Schulten, 1979; Schulten *et al.*, 1984; Tavan *et al.*, 1985). However, the barrier for rotation around the 14—15 bond can be lowered to 5 kcal/mol by deprotonation. After the Asp-85 accepts the Schiff base proton, retinal can isomerize rapidly to the 13-*cis* state presented as the second step in Fig. 10. However, the system is then again trapped since the barrier for rotation around the 13—14 bond for the unprotonated Schiff base is over 20 kcal/mol (Tavan *et al.*, 1985). Protonation of retinal through Asp-96 can lower the intramolecular barrier to about 10 kcal/mol allowing return to the initial all-*trans* state, a reaction shown as the third step in Fig. 10. The nature of the O_{640} intermediate, formed under suitable conditions at this stage, has been discussed in Schulten *et al.* (1984) and Tavan *et al.* (1985). Figures 8 and 10 together demonstrate clearly that the mechanism fits ideally into the structural context of bacteriorhodopsin.

It is of interest to remark at this point that the mechanism discussed and presented in Fig. 10 can also explain Cl^- ion transport as has been argued in Oesterhelt *et al.* (1986). For this purpose, instead of deprotonating the retinal Schiff base, a Cl^- ion is bound and, instead of protonating the retinal Schiff base, the Cl^- ion is removed. One would then expect that bacteriorhodopsin can also function as a Cl^- ion pump under circumstances which prevent deprotonation, *i.e.*, at very low pH. A contribution by Kesthelyi *et al.* (1991), which demonstrates a light-induced Cl^- ion current, provides remarkable support for the suggested mechanism.

The availability of the structure of a retinal protein opens the door to a wide range of new studies,

molecular dynamics investigations most likely being among the most interesting opportunities. We like to comment briefly on the prospects for such investigations. Clearly these prospects will depend foremost on the availability of an improved experimental structure since the molecular dynamics method is far from allowing a reliable prediction of missing structural elements of proteins. However, if one wants to determine the mechanism of proton pumping, the requirements on the pertinent structural data are very high, *e.g.*, one needs to identify water and hydrogen bonds in the protein and one would also need short time resolution methods to observe structural changes accompanying the BR → L → M transitions. Thus, one can safely predict that, even if greatly improved structural information will be available, molecular dynamics simulations will still have to fill in many information gaps for an understanding of the mechanisms of retinal proteins to be achieved.

Presently, without further structural information at hand, the following investigations appear to be most desirable. First, one should attempt to place water into bacteriorhodopsin since it is well-known that about 10 water molecules are located in the vicinity the retinal binding site. One should also extend the time scale of the simulations; only about 50 ps were covered in the present simulation, excluding 100 ps of equilibration. One especially crucial consequence of the involvement of a primary all-*trans* → 13,14-*dicis* photo-isomerization in the mechanism of proton pumping needs to be tested: does retinal spontaneously, *i.e.*, within about 1 ns, assume a 13-*cis* isomeric state after the initial isomerization and deprotonation (deprotonation lowering the barrier for rotation around the 14—15 bond)? Another consequence to be tested is whether retinal, the barrier of rotation around its 13—14 bond being lowered, assumes again an all-*trans* form. Presently, simulation of such a process is beyond the time horizon, about 10 ns, of molecular dynamics methods. The process might be speeded-up by eliminating said barrier altogether, but it is by no means certain that this suffices for a 10 ns isomerization to yield an all-*trans* isomer. Another question which can possibly be answered by means of molecular dynamics simulations is the nature of the forces, *i.e.*, sterical, Coulombic, entropic, which drive the proton pump cycle of bacteriorhodopsin, a topic discussed in Schulten *et al.* (1984).

An understanding of the proton pump mechanism will require also a proper description of the p*K*-values of groups involved in the proton conduction pathway and in the control of the protonation state of the retinal chromophore. Such a description requires one to determine the electrostatic field inside the protein. This field will also contribute to the large spectral shifts experienced by retinal. These shifts have been calculated in the past, but a renewed effort in light of the Henderson model quickly revealed that it has been much easier to "predict" these shifts without a structure than it is now with a structure at hand. Factors like local anisotropic polarizabilities and exact placement of ions and water are likely to have a profound influence on retinal spectral shifts.

Preliminary investigations have shown that the interaction between the protonated and unprotonated Schiffbase nitrogen with the protonated and unprotonated counterions Asp-212 and Asp-85 is a key determinant for the stereochemistry of retinal during the proton pump cycle of bacteriorhodopsin.

Ultimately, one wants to describe the function and properties of bacteriorhodopsin in its native membrane–water environment. The rapid development of concepts and algorithms for molecular dynamics simulations, in particular improved long time scale simulation methods, and the enormous increase of computational capacities through parallel machines (the present study relied on one such machine, the Connection Machine CM-2), will likely allow us to reach this goal and to reach a new level of understanding of metabolism and of biological vision.

Acknowledgements—One of the authors (K.S.) wishes to thank Walter Stoeckenius for sharing unselfishly over many years his broad knowledge, deep insight and continuous excitement and for paving a theoretical physicist's way into a challenging and beautiful area of biology. This research has been carried out at the Center for Parallel Computation in Molecular Dynamics funded by the National Institutes of Health. M.N. gratefully acknowledges financial support by the Kanton Zürich, Switzerland. A.W. would like to thank the Böhringer Ingelheim Fonds of Stuttgart, Fed. Rep. Germany for their support. We thank the staff of the National Center for Supercomputing Applications and of Thinking Machines Corporation for their assistance. The computations were done on a 32K processor Connection Machine CM-2 and on a Cray-2 at the National Center for Supercomputer Applications supported by the National Science Foundation.

REFERENCES

Aton, B., A. G. Doukas, R. H. Callender, B. Becker and T. G. Ebrey (1977) Resonance raman studies of the purple membrane. *Biochemistry* **16**, 2995–2999.

Berendsen, H., J. Postma, W. van Gunsteren and J. Hermans (1984) Coupling to a heat bath. *J. Chem. Phys.* **81**, 3684.

Braiman, M. S., T. Mogi, T. Marti, L. J. Stern, H. G. Khorana and K. J. Rothschild (1988) Vibrational spectroscopy of bacteriorhodopsin mutants: light-driven proton transport involves protonation changes of aspartic acid residues 85, 96, and 212. *Biochemistry* **27**, 8516–8520.

Brooks, B. R., R. E. Bruccoleri, B. D. Olafson, D. J. States, S. Swaminathan, and M. Karplus (1983) CHARMM: a program for macromolecular energy minimization and dynamics calculations. *J. Comput. Chem.* **4**, 187–217.

Brünger, A. T. (1988) Crystallographic refinement by simulated annealing. In *Crystallographic Computing 4: Techniques and New Technologies* (Edited by N. W. Isaacs and M. R. Taylor). Clarendon Press, Oxford.

Dewar, M. J. S. and J. J. P. Stewar (1986) AMPAC. *Quant. Chem. Program Exch. Bull.* **6**, 24.

Dobler, J., W. Zinth, W. Kaiser and D. Oesterhelt (1988) Excited-state reaction dynamics of bacteriorhodopsin studied by femtosecond spectroscopy. *Chem. Phys. Lett.* **144**, 215–220.

Fahmy, K., F. Siebert, M. F. Grossjean and P. Tavan (1989) Photoisomerization in bacteriorhodopsin studied by FTIR, Linear dichroism and photoselection experiments combined with quantum chemical theoretical analysis. *J. Mol. Struct.* **214**, 257–288.

Fodor, S. P. A., J. B. Ames, R. Gebhard, E. M. M. van den Berg, W. Stoeckenius, J. Lugtenburg and R. A. Mathies (1988a) Chromophore structure in bacteriorhodopsin's N intermediate: implications for the proton-pumping mechanism. *Biochemistry* **27**, 7097–7101.

Fodor, S. P. A., W. T. Pollard, R. Gebhard, E. M. M. van den Berg, J. Lugtenburg and R. A. Mathies (1988b) Bacteriorhodopsin's L_{550} intermediate contains a C14—C15 s-*trans*-retinal chromophore. *Proc. Natl. Acad. Sci. USA* **85**, 2156–2160.

Gerwert, K., B. Hess, J. Soppa and D. Oesterhelt (1989) Role of Asp-96 in proton translocation by bacteriorhodopsin. *Proc. Natl. Acad. Sci. USA* **86**, 4943–4947.

Grossjean, M. F., P. Tavan and K. Schulten (1980) Quantum chemical vibrational analysis of the chromophore of bacteriorhodopsin. *J. Phys. Chem.* **94**, 8059–8069.

Grossjean, M. F., P. Tavan and K. Schulten (1989) Can normal mode analysis reveal the geometry of the L_{550} chromophore of bacteriorhodopsin? *Eur. Biophys. J.* **16**, 341–349.

Harbison, G. S., S. O. Smith, J. A. Pardoen, J. M. L. Courtin, J. Lugtenburg, J. Herzfeld, R. A. Mathies and R. G. Griffin (1985) Solid-state ^{13}C NMR detection of a perturbed 6-s-*trans* chromophore in bacteriorhodopsin. *Biochemistry* **24**, 6955–6962.

Henderson, R. (1977) The purple membrane from halobacterium halobium. *Annu. Rev. Biochem. Bioeng.* **6**, 87–109.

Henderson, R., J. M. Baldwin, T. A. Ceska, F. Zemlin, E. Beckmann and K. H. Downing (1990) Model for the structure of bacteriorhodopsin based on high-resolution electron cryo-microscopy. *J. Mol. Biol.* **213**, 899–929.

Honig, B., B. Hudson, B. D. Sykes and M. Karplus (1971) Ring orientation in β-ionone and retinals. *Proc. Natl. Acad. Sci. USA* **68**, 1289–1293.

Karplus, M. (1986) Molecular dynamics of proteins. In *Structure and Dynamics of Nucleic Acids, Proteins and Membranes* (Edited by E. Clementi and S. Chin) pp. 113–126. Plenum Press, London.

Keszthelyi, L. and P. Ormos (1980) Electrical signals associated with the photocycle of bacteriorhodopsin. *FEBS Lett.* **109**, 189–193.

Lin, S. W. and R. A. Mathies (1989) Orientation of the protonated retinal schiff base group in bacteriorhodopsin from absorption linear dichroism. *Biophys. J.* **56**, 653–660.

Lozier, R. H., Bogomolni, R. A. and W. Stoeckenius (1975) Bacteriorhodopsin: a light-driven proton pump in halobacterium halobium. *Biophys. J.* **15**, 955–962.

Mathies, R. A., C. H. B. Cruz, W. T. Pollard and C. V. Shank (1988) Direct observation of the femtosecond excited state *cis-trans* isomerization in bacteriorhodopsin. *Science* **240**, 777–779.

Mitchell, P. (1961) Coupling of phosphorylation to electron and hydrogen transfer by a chemi-osmotic type of mechanism. *Nature* **191**, 144–148.

Nakanishi, K., V. Balog-Nair, M. Arnaboldi, K. Tsujimoto and B. Honig (1980) An external point-charge model for bacteriorhodopsin to account for its purple color. *J. Am. Chem. Soc.* **102**, 7945–7947.

Nonella, M. and K. Schulten (1991) Molecular dynamics simulation of electron transfer in proteins—theory and application to $Q_A \rightarrow Q_B$ transfer in the photosynthetic reaction center. *J. Phys. Chem.* **95**, 2059–2067.

Oesterhelt, D. (1976) Bacteriorhodopsin as an example of a light-driven proton pump. *Angew. Chem. Int. Ed. Engl.* **15**, 16–24.

Oesterhelt, D., P. Hegemann, P. Tavan and K. Schulten (1986) *Trans–cis* isomerization of retinal and a mechanism for ion translocation in halorhodopsin. *Eur. Biophys. J.* **14**, 123–129.

Oesterhelt, D. and W. Stoeckenius (1973) Functions of a new photoreceptor membrane. *Proc. Natl. Acad. Sci. USA* **70**, 2853–2857.

Orlandi, G. and K. Schulten (1979) Coupling of stereochemistry and proton donor-acceptor properties of a schiff base: a model of a light-driven proton pump. *Chem. Phys. Lett.* **64**, 370–374.

Pettei, M. J., A. P. Yudd, K. Nakanishi, R. Henselman and W. Stoeckenius (1977) Identification of retinal isomers isolated from bacteriorhodopsin. *Biochemistry* **16**, 1955–1959.

Polygen (1988) *Quanta*. Polygen Corp., 200 Fifth Ave., Waltham, MA 02254, USA.

Schulten, K. (1978) An isomerization model for the photocycle of bacteriohodopsin. In *Energetics and Structure of Halophilic Microorganism* (Edited by S. R. Caplan and M. Ginzburg), pp. 331–334. Elsevier, Amsterdam.

Schulten, K., Z. Schulten and P. Tavan (1984) An isomerization model for the pump cycle of bacteriorhodopsin. In *Information and Energy Transduction in Biological Membranes* (Edited by L. Bolis, E. J. M. Helmreich and H. Passow), pp. 113–131. Alan R. Liss, New York.

Schulten, K. and P. Tavan (1978) A mechanism for the light-driven proton pump of halobacterium halobium. *Nature* **272**, 85–86.

Smith, S. O., I. Hornung, R. van der Steen, J. A. Pardoen, M. S. Braiman, J. Lugtenburg and R. Mathies (1986) Are C14—C15 single bond isomerizations of the retinal chromophore involved in the proton-pumping mechanism of bacteriorhodopsin? *Proc. Natl. Acad. Sci. USA* **83**, 967.

Tavan, P., K. Schulten and D. Oesterhelt (1985) The effect of protonation and electrical interactions on the stereochemistry of retinal schiff bases. *Biophys. J.* **47**, 415–430.

Treutlein, H., K. Schulten, J. Deisenhofer, H. Michel, A. Brünger and M. Karplus (1988) Molecular dynamics simulation of the primary processes of the photosynthetic reaction center of rhodopseudomonas viridis. In *The Photosynthetic Bacterial Reaction Center: Structure and Dynamics* (Edited by J. Breton and A. Vermeglio), pp. 139–150. Plenum Press, London.

Windemuth, A. and K. Schulten (1991) Molecular dynamics on the Connection Machine. *Mol. Simul.* **5**, 353–361.